International Forum on Aeroelasticity and Structural Dynamics
IFASD 2024
17-21 June 2024, The Hague, The Netherlands

GUST RESPONSE ANALYSIS OF SUPERSONIC AIRCRAFT BASED ON THREE-DIMENSIONAL PISTON THEORY

Chen Song, Changchuan Xie*, Chenyu Liu, Yang Meng

Beihang University
Xueyuan Road 37, 100191 Beijing, China
18351049@buaa.edu.cn
xiechangc@buaa.edu.cn
lcy@buaa.edu.cn
summy@buaa.edu.cn

Keywords: piston theory, supersonic, aeroelasticity, gust response

Abstract: The piston theory is a highly efficient method used for supersonic aerodynamic calculations at Ma>2.5. This study applies first-order piston theory to a three-dimensional surface mesh to derive the generalized aerodynamic influence coefficient (AIC) matrix, which can be separated into aerodynamic stiffness and damping. By employing a tightly coupled aeroelastic model, the modal response of the structure to gusts can be analytically solved in the frequency domain or semi-analytically in the time domain while the current solution relies on rational function approximation and ODE solvers.

1 INTRODUCTION

Though extensive research has been conducted on the impact of atmospheric disturbances (gusts) on low-speed aircraft since the Helios Prototype incident [1], there is still a need for further exploration of gust loads on supersonic vehicles, as well as the development of efficient analysis methods [2]. Additionally, the emergence of hypersonic glide vehicles has highlighted that the integration of warheads and boosters typically operates at a lower fundamental frequency compared to supersonic fighters, making them more susceptible to atmospheric disturbances. Therefore, it is essential to examine the gust response of supersonic aircraft.

As an efficient supersonic unsteady aerodynamic method, the piston theory was first proposed by M.J. Lighthill [3] in the 1950s and became one of the most practical methods for supersonic aeroelastic analysis with further development by H. Ashley [4] and others. C. Mei [5] used piston theory to analyze the nonlinear flutter of wall panels, and P.P. Fredmann [6] systematically compared the differences in flutter analysis between piston theory and the Navier-Stokes equations.

In recent years, Linear-theory-based lifting-surface methods have become popular due to the success of the ZONA51 [7] and ZONA51U code [8], which has good consistency with experiments in flutter speed but needs extra treatments including rational approximation [9] or inverse Fourier transformation to obtain the time-domain response. On the other hand, both the accuracy and range of application of piston theory could be improved with the steady local tangential speed of the vehicle surface calculated by CFD. This new method called local piston theory [10,11] holds the precision of unsteady CFD with the computation overhead of one steady CFD and, therefore becomes preferable for aeroelastic analysis in the time domain though the present research focuses mainly on airfoil and thin wing.

In this paper, the first-order piston theory is applied to the 3D grid of arbitrary vehicle surfaces so that the unsteady aerodynamic force caused by structural deformation can be described linearly with the aerodynamic influence coefficient (AIC) matrix, which makes it possible to solve the aeroelastic system's dynamic response analytically in both frequency domain and time domain.

2 CALCULATION OF AERODYNAMIC FORCE

With the finite element mode superposition method, this paper presents the unsteady aerodynamic force resulting from structural vibration in matrix form. While this chapter utilizes classic piston theory, the same approach can be applied to local piston theory by substituting the incoming flow parameters with the local parameter of the mean steady flow field determined by CFD.

2.1 Piston theory for 3D mesh

Classic piston theory is a strictly one-dimensional quasi-steady theory which holds that the disturbance pressure at a point on the surface of an object in supersonic airflow is only related to the downwash velocity at that point [10], as shown in the diagram below:

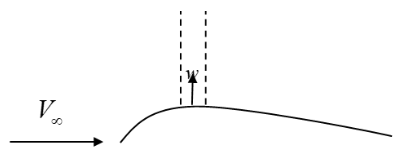

Figure 1: The schematic of classic piston theory

where V_∞ represents the velocity of the incoming flow and w is the downwash speed at surface points. Approximating the propagation of disturbances along the normal to the surface as the adiabatic expansion of gas in a one-dimensional piston, the reactive force of the gas on the surface can be obtained based on the principle of momentum [2]:

$$p = p_\infty \left(1 + \frac{\gamma - 1}{2} \frac{w}{a_\infty}\right)^{\frac{2\gamma}{\gamma-1}} \tag{1}$$

Where p_∞, a_∞, and γ represent velocity, speed of sound, and specific heat ratio of the incoming flow respectively. The first-order piston theory only adopts the first term of Eq.(1) using Taylor expansion and holds:

$$\begin{aligned} p &= p_\infty + \rho_\infty a_\infty w \\ \Delta P &= P - P_\infty = \rho_\infty a_\infty w \end{aligned} \tag{2}$$

With ρ_∞ being the density of incoming flow.

To apply the above equation to 3D vehicle surfaces, a local coordinate system $P\xi\eta\zeta$ is established on the tangent plane of the surface at point P, where ξ denotes the projection of the incoming flow on the tangent plane, ζ the normal direction pointing outwards, and η determined by the right-hand rule.

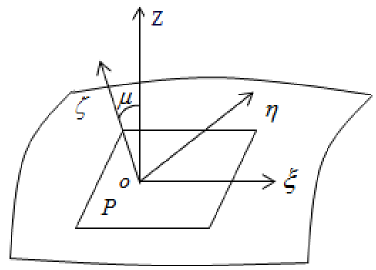

Figure 2: The tangent plane and local coordinate system at point P [12]

With $\boldsymbol{w}_a(x,y,z,t)$ denotes the deformation of any point on the aerodynamic mesh and $\boldsymbol{n}(x,y,z)$ the corresponding normal direction, the downwash speed w should be replaced with normal wash speed w_n that could be expressed at the global coordinate Oxyz as:

$$\begin{aligned} w_n &= \mathbf{n}^T \frac{d}{dt}\boldsymbol{w}_a - V_\zeta \\ &= \mathbf{n}^T \left(\frac{\partial \boldsymbol{w}_a}{\partial t} + \frac{\partial \boldsymbol{w}_a}{\partial \xi} V_\xi - \boldsymbol{V}_\infty \right) \end{aligned} \tag{3}$$

In Eq.(3), $\boldsymbol{V}_\infty$ is the velocity vector of the incoming flow at three-dimensional space and V_ξ is its tangential component. Notice that only the first two terms represent unsteady disturbances caused by the structure's vibration, while the last term represents the steady component.

2.2 Deflection interpolation and AIC

In the assumption of small perturbation, the structure's elastic deformation $\boldsymbol{w}_s$ can be expressed with the mode superposition method [13]:

$$\boldsymbol{w}_s(x_i, y_i, z_i, t) = \boldsymbol{\Phi}_i \boldsymbol{q}(t) \tag{4}$$

where $\boldsymbol{\Phi}_i$ represents the modal matrix at point (x_i, y_i, z_i) and $\boldsymbol{q}(t)$ the general coordinate. Since the aerodynamic meshes do not coincide with the structural finite elements' surface grids in most cases, surface spline interpolation is adopted to interpolate the structural modes onto the aerodynamic mesh.

Though the infinite-plate spline [14] (IPS) and its 3D form, thin-plate spline [15] (TPS) have become the standard method in aeroelastic analysis [16], a further generalization of TPS is exploited in this paper to obtain both the displacement mapping and tangent mapping [17] with preferable accuracy and fitting smoothness [18].

With a set of structural surface points $\boldsymbol{x}_1 \sim \boldsymbol{x}_N$, the following spline function holds:

$$\boldsymbol{w}(\boldsymbol{x}) = \boldsymbol{c}_0 + \mathbf{C}_1\boldsymbol{x} + \sum_{i=1}^{N} \boldsymbol{c}_{i+1} r_i^2 \ln(r_i^2 + \varepsilon) \tag{5}$$

where $r_i = \|\boldsymbol{x} - \boldsymbol{x}_i\|$ and hyperparameter $\varepsilon = 10^{-2} \sim 1$ for smooth function. The other undetermined coefficients in Eq.(5) are obtained by solving the following linear equations:

$$\begin{cases} \sum_{i=1}^{N} \mathbf{c}_{i+1} = \mathbf{0} \\ \sum_{i=1}^{N} \boldsymbol{x}_i \otimes \boldsymbol{c}_{i+1} = \mathbf{0} \\ \boldsymbol{w}(\boldsymbol{x}_i) = \mathbf{\Phi}_i \boldsymbol{q}(t) \end{cases} \tag{6}$$

Based on the spline function above, the interpolation mapping from structural displacement and the deformation of aerodynamic grids could be written in matrix form [17]:

$$\boldsymbol{w}_a(x, y, z, t) = \mathbf{P}(x, y, z)\mathbf{\Phi}_s \boldsymbol{q}(t) \tag{7}$$

where $\mathbf{P}$ is the transformation matrix of interpolation defined by the position of the given structural grids $\boldsymbol{x}_1 \sim \boldsymbol{x}_N$ and $\mathbf{\Phi}_s$ represents the modal matrix of the given structural grids.

With modal spline interpolation, Eq.(3) could be rewritten using general coordinates:

$$w_n = \boldsymbol{n}^T \left(\mathbf{P}\mathbf{\Phi}_s \dot{\boldsymbol{q}} + V_\xi (\nabla \xi)^T (\nabla \mathbf{P}) \mathbf{\Phi}_s \boldsymbol{q} - \boldsymbol{V}_\infty \right) \tag{8}$$

where $\nabla(\cdot) = \begin{bmatrix} \frac{\partial(\cdot)}{\partial x} & \frac{\partial(\cdot)}{\partial y} & \frac{\partial(\cdot)}{\partial y} \end{bmatrix}^T$ is the gradient operator. It's clear that the unsteady component of w_n has two sources: $\dot{\boldsymbol{q}}$ and $\boldsymbol{q}$, corresponding to aerodynamic damping and aerodynamic stiffness respectively. Furthermore, the unsteady component of Eq.(8) also applies to local piston theory with V_ξ replaced with the local tangential speed of the mean steady flow field determined by CFD.

Considering the discretized aerodynamic mesh, the aerodynamic force on a single element could be expressed as:

$$\Delta \boldsymbol{F}_i = \Delta p_i s_i \boldsymbol{n}_i \tag{9}$$

where Δp_i, s_i, $\boldsymbol{n}_i$ represent the pressure, area, and normal direction of the ith element.

Apply Eq.(2) and Eq.(8) to Eq.(9), the aerodynamic force acting on the aerodynamic mesh could be written in matrix form:

$$\boldsymbol{F}_a = \begin{bmatrix} \Delta \boldsymbol{F}_1 \\ \vdots \\ \Delta \boldsymbol{F}_{N_a} \end{bmatrix} = \mathbf{A}_0 \dot{\boldsymbol{q}} + \mathbf{A}_1 \boldsymbol{q} + \boldsymbol{F}_{origin} \tag{10}$$

where N_a is the total number of aerodynamic grids and the parameters $\mathbf{A}_0, \mathbf{A}_1, \boldsymbol{F}_{origin}$ are determined only by the structure's discretization model and incoming flow parameters.

In dynamic response analysis, only the unsteady aerodynamic force component is significant, represented by the general aerodynamic influence coefficient (AIC) matrix:

$$\begin{aligned} \mathbf{C}_a &= \mathbf{\Phi}_a^T \mathbf{A}_0 \\ \mathbf{K}_a &= \mathbf{\Phi}_a^T \mathbf{A}_1 \end{aligned} \tag{11}$$

where $\mathbf{\Phi}_a$ is the mapping of $\mathbf{\Phi}_s$ to the aerodynamic mesh following Eq.(7) :

$$\mathbf{\Phi}_a = \begin{bmatrix} \mathbf{P}_1 \\ \vdots \\ \mathbf{P}_{N_a} \end{bmatrix} \mathbf{\Phi}_s \tag{12}$$

$\mathbf{P}_i, i = 1, 2, \cdots N_a$ is the transformation matrix of interpolation corresponding to the i$^{\text{th}}$ aerodynamic element.

2.3 Generalized aerodynamic force induced by Gust

Considering the general model of discrete gust shown below:

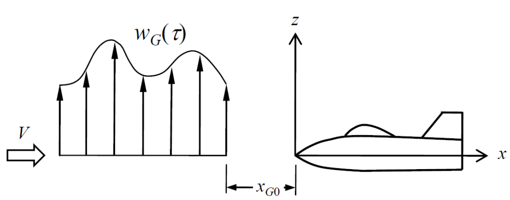

Figure 3: Diagram of discrete gust

where x is the direction of the incoming flow and $\tau = t - \frac{x - x_{G_0}}{V_\infty}$ represents the "local time" influenced by the aircraft's scale and movement. $w_G(t)$ is the discrete gust model, the most common forms of which are step gust and "1-cos" gust [19] defined in the time domain as follows:

Step gust:

$$w_G(t) = \omega_m \cdot u(t) \tag{13}$$

where ω_m is the amplitude and $u(t)$ is the unit step function.

One minus cos gust:

$$w_G(t)=\frac{\omega_m}{2}\left(1-\cos\frac{2\pi\left|\boldsymbol{V}_\infty\right|t}{L}\right)\left(u(t)-u(t-\frac{L}{\left|\boldsymbol{V}_\infty\right|})\right) \tag{14}$$

where L represents the gust scale.

The gust disturbance applied on the aerodynamic mesh is:

$$\begin{gathered}\boldsymbol{w}_{\mathrm{G}}\left(t\right)=\left[w_1\left(t\right)\ldots w_{N_a}\left(t\right)\right]^T\\ w_i=w_G(t-\frac{x_i-x_{G_0}}{V_\infty}),i=1,2,\cdots N_a\end{gathered} \tag{15}$$

with flow-wise coordinate x_i defined as the projection of the aerodynamic grid centroids' position vector $\boldsymbol{r}_i$ on $\hat{\boldsymbol{v}}$, the direction of the incoming flow.

$$\begin{bmatrix}x_1\\ \vdots\\ x_{N_a}\end{bmatrix}=\begin{bmatrix}\boldsymbol{r}_1 & \cdots & \boldsymbol{r}_{N_a}\end{bmatrix}^{\mathrm{T}}\hat{\boldsymbol{v}} \tag{16}$$

Then the aerodynamic force caused by gust disturbance could be obtained by substituting Eq.(15) and Eq.(2) into Eq.(9):

$$\boldsymbol{F}_{\text{gust}}\left(\mathrm{t}\right)=\begin{bmatrix}\boldsymbol{F}_1\\ \vdots\\ \boldsymbol{F}_{N_a}\end{bmatrix}=\begin{bmatrix}\rho_1 a_1 s_1 w_1\left(t\right)\boldsymbol{n}_1^T\hat{\boldsymbol{v}}_n\boldsymbol{n}_1\\ \vdots\\ \rho_{N_a}a_{N_a}s_{N_a}w_{N_a}\left(t\right)\boldsymbol{n}_{N_a}^T\hat{\boldsymbol{v}}_n\boldsymbol{n}_i\end{bmatrix} \tag{17}$$

where $\hat{\boldsymbol{v}}_n$ is the direction of the gust profile, which is usually perpendicular to the incoming flow. Notice that Eq.(17) uses the local flow parameter at each grid and therefore applies to both the classic piston theory and local piston theory. For classic piston theory, the equation could be simplified with $\rho_i a_i=\rho_\infty a_\infty$.

With the mapping of the modal matrix defined in Eq.(12), the generalized force caused by gust disturbance is simply obtained:

$$\boldsymbol{Q}_{\text{gust}}=\boldsymbol{\Phi}_a^T\boldsymbol{F}_{\text{gust}} \tag{18}$$

3 DYNAMIC MODELING AND SOLUTION

In this section, the equations of aeroelasticity are established based on the small perturbation and deformation assumptions of linear elasticity, providing both semi-analytical solutions in the time domain and analytical solutions in the frequency domain.

3.1 State-space equations and their solution in the time domain

Denote the general mass, damping, and stiffness matrix of the structure as $\mathbf{M}, \mathbf{C}_s, \mathbf{K}_s$ respectively, the structural dynamic equation has the following form [11]:

$$\mathbf{M}\ddot{\boldsymbol{q}} + \mathbf{C}_s\dot{\boldsymbol{q}} + \mathbf{K}_s\boldsymbol{q} = \mathbf{C}_a\dot{\boldsymbol{q}} + \mathbf{K}_a\boldsymbol{q} + \boldsymbol{Q}_{gust} \tag{19}$$

Set the state quantity to be $\boldsymbol{y} = [\dot{\boldsymbol{q}}^T \quad \boldsymbol{q}^T]^T$ and let $\mathbf{K} = \mathbf{K}_s - \mathbf{K}_a$, $\mathbf{C} = \mathbf{C}_s - \mathbf{C}_a$, Eq.(19) could be rewritten in the state space:

$$\dot{\boldsymbol{y}} = \begin{bmatrix} -\mathbf{M}^{-1}\mathbf{C} & -\mathbf{M}^{-1}\mathbf{K} \\ \mathbf{I} & \mathbf{0} \end{bmatrix} \boldsymbol{y} + \begin{bmatrix} \mathbf{M}^{-1}\boldsymbol{Q}_{gust} \\ \boldsymbol{0} \end{bmatrix} \tag{20}$$

or simply

$$\dot{\boldsymbol{y}}(t) = \mathbf{A}\boldsymbol{y}(t) + \boldsymbol{f}(t) \tag{21}$$

with analytical solution [20]:

$$\begin{aligned} \boldsymbol{y}(t) &= \boldsymbol{\psi}(t)\left[\boldsymbol{\psi}^{-1}(t_0)\boldsymbol{y}_0 + \int_{t_0}^{t} \boldsymbol{\psi}^{-1}(s)\boldsymbol{f}(s)\,ds\right] \\ \boldsymbol{\psi}(t) &= e^{\mathbf{A}t} \end{aligned} \tag{22}$$

Where $\boldsymbol{y}(t_0) = \boldsymbol{y}_0$ is the initial condition.

In practice, the definite integral in Eq.(22) should be solved numerically, therefore providing a semi-analytical solution: assuming $t_0 = 0$ and a discrete time series $t_k = k\Delta t$, Eq. (22) could be solved recurrently:

$$\boldsymbol{y}(t_k) = \begin{cases} \boldsymbol{y}_0 & k = 0 \\ \boldsymbol{\psi}(\Delta t)\,\boldsymbol{y}(t_{k-1}) + \int_{t_{k-1}}^{t_k} \boldsymbol{\psi}(t_k - s)\,\boldsymbol{f}(s) & else \end{cases} \tag{23}$$

Solving Eq.(23) with numerical integration methods like Simpson's rule has advantages against solving Eq.(21) directly with ODE solvers in numerical stability and efficiency, which could be enlarged further with advanced methods[21] for the computation of exponential matrix $\boldsymbol{\psi}(t)$.

3.2 Frequency domain solution

Apply Fourier transform on Eq.(15), the time-shift effect caused by the aircraft's scale and movement is represented equivalently in the frequency domain as:

$$W_i(j\omega) = W_G(j\omega)e^{-j\omega\left(\frac{x_i - x_0}{V_\infty}\right)} \tag{24}$$

where $W_G(j\omega) = \mathcal{F}\{w_G(t)\}$ is the Fourier transform of the gust profile.

In this paper, the Fourier transform of discrete gusts are derived utilizing Laplace transform with the following results:

Step gust:

$$W_G(j\omega) = \frac{\omega_m}{j\omega} \tag{25}$$

One minus cos gust:

$$W_G(j\omega) = \frac{\omega_m}{2}\left(\frac{4\pi^2 V_\infty{}^2}{j\omega(4\pi^2 V_\infty{}^2 - L^2\omega^2)}\right)\left(1 - e^{-\frac{j\omega L}{V_\infty}}\right) \tag{26}$$

with the same parameters as the time domain expression.

Similarly, the aerodynamic force caused by the gust can be expressed in the frequency domain by taking the Fourier transform of Eq.(17):

$$\mathcal{F}\{\boldsymbol{F}_{\text{gust}}(t)\} = \begin{bmatrix} \rho a s_1 e^{-j\omega\left(\frac{x_1 - x_0}{V_\infty}\right)} \boldsymbol{n}_1^T \hat{\boldsymbol{v}}_n \boldsymbol{n}_1 \\ \vdots \\ \rho a s_{N_a} e^{-j\omega\left(\frac{x_{N_a} - x_0}{V_\infty}\right)} \boldsymbol{n}_{N_a}^T \hat{\boldsymbol{v}}_n \boldsymbol{n}_i \end{bmatrix} W_G(j\omega) \tag{27}$$

or simply $\mathcal{F}\{\mathbf{F}_{\text{gust}}(t)\} = \mathbf{A}_g W_G(j\omega)$ with $\mathbf{A}_g$ being the AIC matrix of gust. The zero-state frequency domain response can be analytically calculated from the Fourier transform of Eq.(19):

$$\mathcal{F}\{\boldsymbol{q}(t)\} = \left[-\omega^2\mathbf{M} + j\omega\mathbf{C} + \mathbf{K}\right]^{-1} \mathbf{\Phi}_a^T \mathbf{A}_g W_G(j\omega) \tag{28}$$

The frequency domain response with initial condition $\boldsymbol{q}(t=0) = \boldsymbol{q}_0$ and $\dot{\boldsymbol{q}}(t=0) = \dot{\boldsymbol{q}}_0$ coulde be derived using Laplace transform:

$$\mathcal{F}\{\boldsymbol{q}(t)\} = \left[-\omega^2\mathbf{M} + j\omega\mathbf{C} + \mathbf{K}\right]^{-1} \left[\mathbf{\Phi}_a^T \mathbf{A}_g W_G(j\omega) + \mathrm{j}\omega\mathbf{M}\boldsymbol{q}_0 + \mathbf{M}\dot{\boldsymbol{q}}_0 + \boldsymbol{q}_0\right] \tag{29}$$

4 NUMERICAL ANALYSIS

In this section, the dynamic responses of a simple wing model under discrete gusts are calculated by both the proposed method and ZAERO to verify the 3D piston theory and semi-analytical solution.

4.1 Structural Model

The shape of the solid wing section used as a verification example is shown in Figure 4 and a finite element model of the wing is built in MSC.Nastran. Mode analysis is performed with its root fixed to obtain the natural frequency and vibration mode of the wing structure.

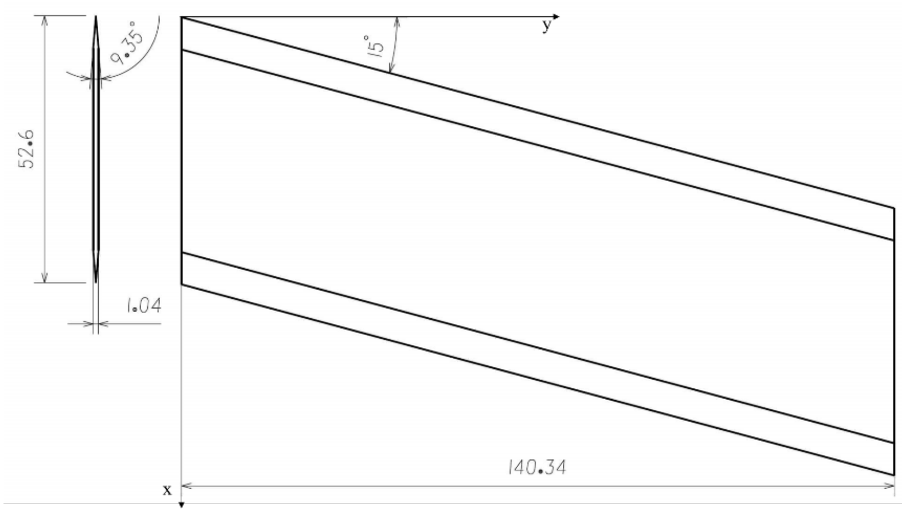

Figure 4: Shape of the wing section in mm

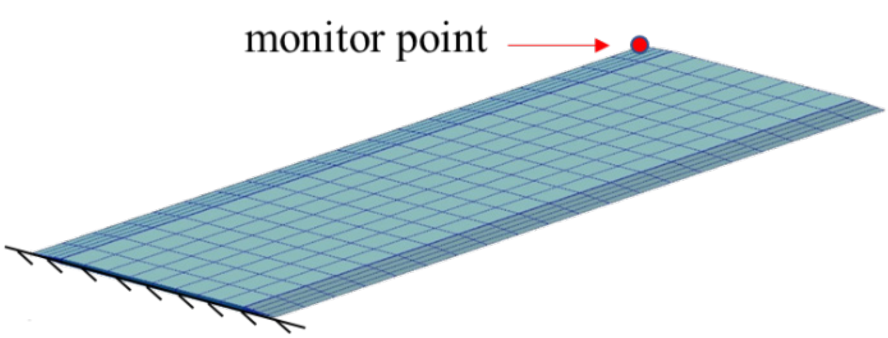

Figure 5: FEM of the wing structure

Properties of the first two modes are shown below: the base frequency is 38.84Hz and the tenth natural frequency is 2461.1Hz.

Table 1: Modal properties of the FE model

Mode	Description	f (Hz)	Modal Shape
1	First bending	38.842	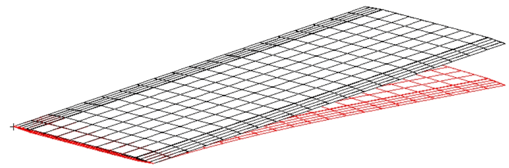
2	First torsion	231.98	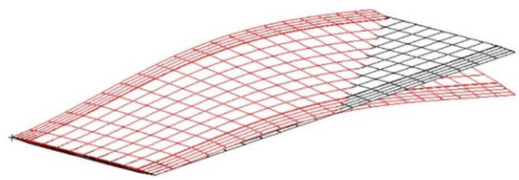

4.2 Calculation Condition

To establish the aeroelastic model, a 3D surface mesh and a 2D projected mesh are used for piston theory and ZONA7U respectively, both sharing the same coordinate system as the structure model. Considering the capability of Zaero, the steady incoming flow is $Ma_\infty = 3.0$ and $V_\infty = 460m/s$ converted according to the dynamic pressure with $\rho_\infty = 1.225kg/m^3$, whose direction coincides with the x axis shown in Figure 4.

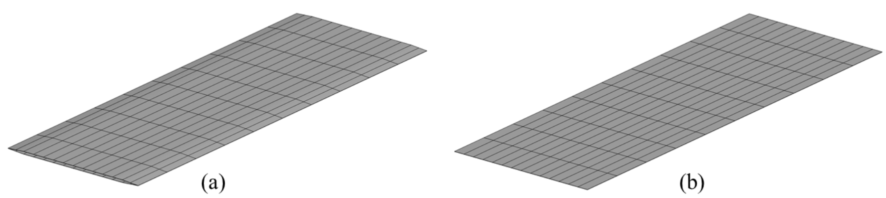

Figure 6: Aerodynamic mesh used: (a) for piston theory; and (b) for Zaero

Both the step gust and "1-cos" gust are used in the verification, with properties shown below:

Table 2: Properties of the discrete gust

Gust type	$x_{G0}(m)$	$\omega_m(m/s)$	$L(m)$
step	20	5	-
1-cos	20	5	12.5

the value of gust scale L for "1-cos" gust is chosen to make its frequency near the structural basic frequency, and the dynamic response would be calculated using the first ten modes of the structure.

4.3 Comparison of Results

In this section, the dynamic response of the wing model under both step and "1-cos" gust are calculated with three methods: Zaero with hybrid approach, the proposed 3D piston theory with Rouge-Kutta method, and 3D piston theory with semi-analytical solution. The z-axial dynamic response of the monitor point located at the leading edge of the wingtip (shown in Figure 5) is used for comparison.

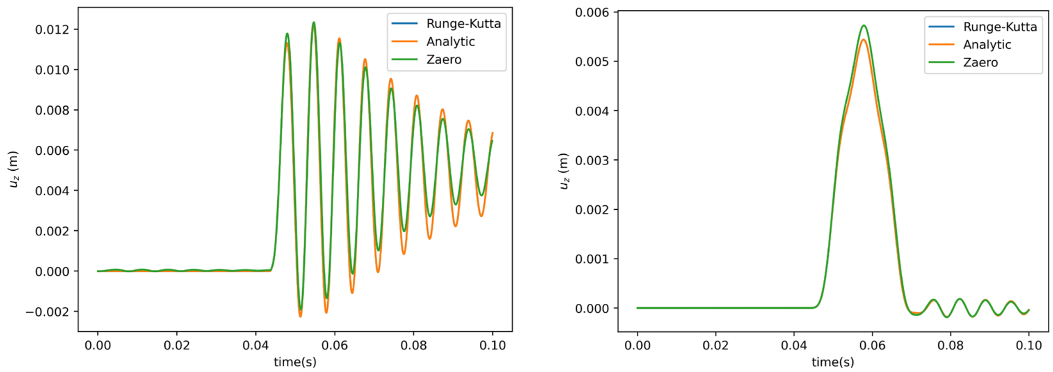

(a) (b)

Figure 7: Displacement response under: (a) step; and (b) “1-cos” gusts

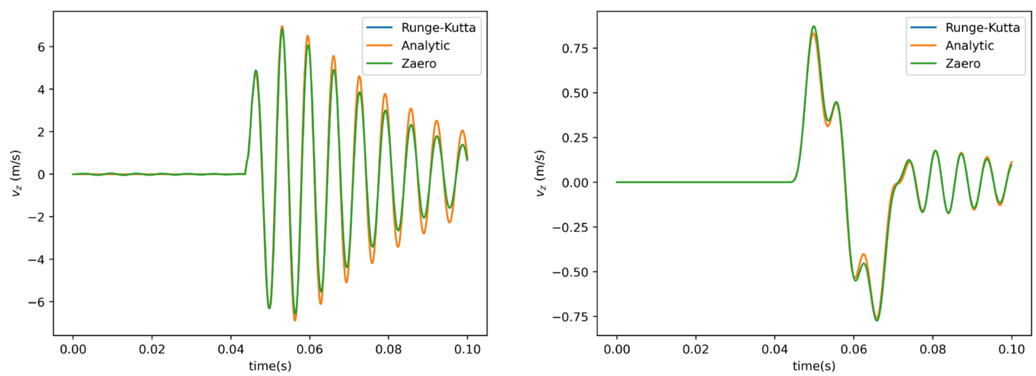

(a) (b)

Figure 8: Velocity response under: (a) step; and (b) “1-cos” gusts

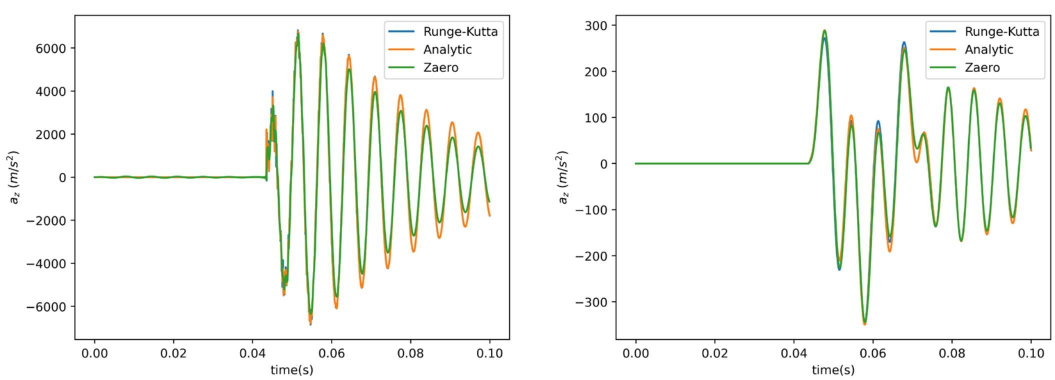

(a) (b)

Figure 9: Acceleration response under: (a) step; and (b) “1-cos” gusts

The calculation results showed astonishing consistency between the three methods. First, the Runge-Kutta method implemented using scipy.integrate.solve_ivp in Python takes 20 times longer than the semi-analytical solution also implemented in Python, yet yields nearly identical results in displacement and velocity responses. It is in the acceleration responses that the difference between

Runge-Kutta method and semi-analytical solution become visible, yet insignificant. Since this paper is not focused on the mathematics of ODE solvers, the source of such differences would not be discussed. Second, the responses calculated using ZONA7U and 3D piston theory holds similar peak values and almost identical vibration frequencies though both the mesh and method for aerodynamic modeling are different. The main difference lays on the aerodynamic damping, which is more obvious in the response of step gust: the vibration amplitude calculated by ZONA7U drops off faster than 3D piston theory.

Table 3: Peak of the responses obtained by both methods

Method	$u_z(mm)$		$v_z(m/s)$		$a_z(m/s^2)$	
	step	1-cos	step	1-cos	step	1-cos
Zaero	12.348	5.727	6.820	0.872	6666.6	288.11
3D piston	12.26	5.440	6.962	0.833	6771.9	289.43
Derivation (%)	-0.71	-5.01	2.08	-4.47	1.58	0.46

Table 3 shows the peak value of the responses obtained by Zaero and semi-analytical solution. It's interesting that the derivation on acceleration is smaller than displacement for "1-cos" gust but larger for step gust, which indicates differences between various solutions at high frequency range.

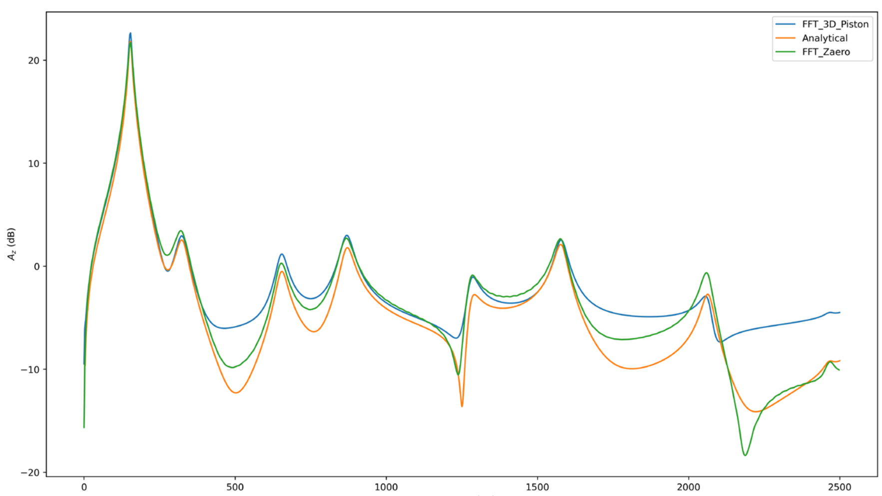

Figure 10: Acceleration response to step gust in frequency domain

In Figure 10, the frequency domain response to step gust given by Eq.(28) is plotted alongside the FFT of the time domain response obtained by Zaero and the semi-analytical solution. It can be seen that though the FFT of time domain solutions have strong consistency with the analytical frequency domain solution, neither of them catches the valley well. Another obvious phenomenon is the relatively high value of FFT_3D_Piston at frequencies greater than 2kHz. This could be due to the algorithms used for exponential matrix and numerical integration, as well as the bit depth used for floating point calculations.

For "1-cos" gust, the results obtained with various methods exhibit strong consistency when the amplitude is greater than -30dB. Similar to the step gust, a relatively high value for FFT_3D_Piston could be observed at frequency greater than 2kHz

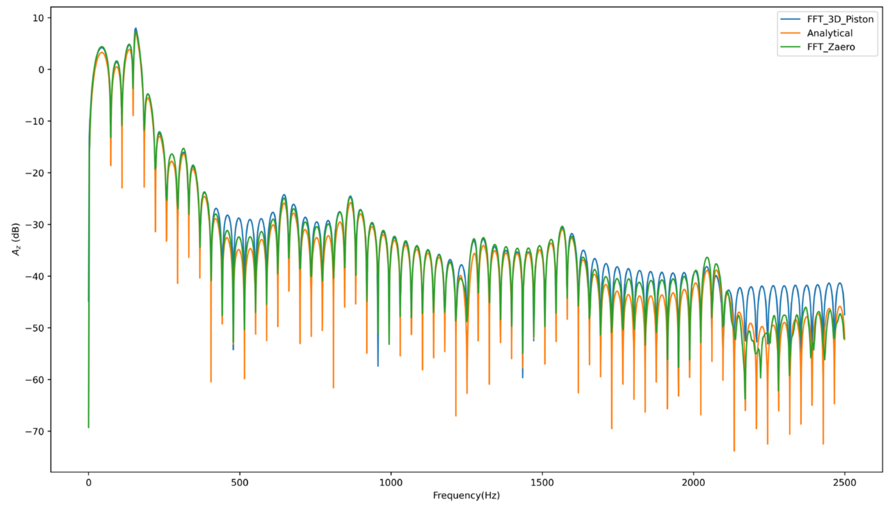

Figure 11: Acceleration response to "1-cos" gust in frequency domain

5 CONCLUSIONS

After been proposed for more than half a century, the classic piston theory is still capable with a few improvements. This paper applies the first order piston theory to discrete 3D surfaces and derives the linear expression of unsteady aerodynamic forces, which is coupled tightly with the structural dynamics model using interpolation techniques to obtain the state-space equation of the aeroelastic system.

By utilizing the method of constant variation, the semi-analytical solution for the time domain response is obtained, proving to be much more efficient compared to ODE solvers. In the frequency domain, the AIC matrix for gust is derived, along with the Fourier transform of discrete gusts, to obtain the analytical solution.

In the numerical example, the proposed method demonstrates acceptable accuracy in both the time and frequency domains. At a higher level, the peak values obtained by both methods have a maximum derivation around 5%, affirming the validity of 3D piston theory. At a more detailed level, the suggested semi-analytical method eliminates the need for converting between frequency and time domains, preserving the high-frequency components effectively. Besides efficiency, another benefit of the proposed method is the separation of time-domain and frequency-domain analyses, thanks to the analytical application of Fourier transform. On the contrary, numerical FFT or IFFT computations are required in panel methods including ZONA7U.

Though the classic piston theory is adopted in this paper, the formulas derived applies to local piston theory as well, which has been demonstrated to overcome the constraints of the classical piston theory concerning flight Mach numbers and angles of attack. Through the 3D generalization of piston theory, conducting rapid dynamic aeroelastic analysis of intricate supersonic vehicles becomes feasible in both time and frequency domain.

REFERENCES

[1] Noll, T. E. and Brown, J. M. and et al. (2004). *Investigation of the Helios Prototype Aircraft Mishap*. Hampton: NASA.

[2] Liu, W. and Zhang, C. A. and Han, H. Q. and et al. (2017). Local Piston Theory with Viscous Correction and Its Application. *AIAA Journal*, 55(3), 942-954.

[3] Lighthill, M. J. (1953). Oscillating Airfoils at High Mach Number. *Journal of the Aeronautical Sciences*, 20(6), 402-406.

[4] Ashley, H. and Zartarian G. (1956). Piston Theory-A New Aerodynamic Tool for the Aeroelastician. *Journal of the Aeronautical Sciences*, 23(12), 1109-1118.

[5] Mei, C. and Abdel-motagaly, K. and Chen, R. (1999). Review of Nonlinear Panel Flutter at Supersonic and Hypersonic Speeds. *Applied Mechanics Reviews*, 52(10), 321-332.

[6] Friedmann, P. P. and Mcnamara, J. J. and Thuruthimattam, B. J. and et al. (2004). Aeroelastic analysis of hypersonic vehicles. *Journal of Fluids and Structures*, 19(5): 681-712.

[7] Liu, D. D. and James, D. K. and Chen, P. C. and et al. (1991). Further studies of harmonic gradient method for supersonic aeroelastic applications. *Journal of Aircraft*, 28(9): 598-605.

[8] Liu, D. D. and Yao, Z. X. and Sarhaddi, D. and et al. (1997). From Piston Theory to a Unified Hypersonic-Supersonic Lifting Surface Method. *Journal of Aircraft*, 34(3): 304-312.

[9] Tiffany, S. and Karpel, M. (1989). Aeroservoelastic modeling and applications using minimum-state approximations of the unsteady aerodynamics. *30th Structures, Structural Dynamics and Materials Conference*. Mobile,AL,U.S.A.: American Institute of Aeronautics and Astronautics.

[10] Zhang, W. W. and Ye, Z. Y. (2005). Numerical method of aeroelasticity based on local piston theory. *Chinese Journal of Theoretical and Applied Mechanics*, 37(5): 632-639.

[11] Zhang, W. W. and Ye, Z. Y. and Zhang, C. A. and et al. (2009). Supersonic Flutter Analysis Based on a Local Piston Theory. *AIAA Journal*, 47(10): 2321-2328.

[12] Liu, C. and Xie, C. and Meng, Y. and et al. (2023). Experimental and Numerical Flutter Analysis Using Local Piston Theory with Viscous Correction. *Aerospace*, 10(10): 870.

[13] Schmidt, D. K. and Raney, D. L. (2001). Modeling and Simulation of Flexible Flight Vehicles. *Journal of Guidance, Control, and Dynamics*, 24(3): 539-546.

[14] Harder, R. L. and Desmarais, R. N. (1972). Interpolation using surface splines. *Journal of Aircraft*, 9(2): 189-191.

[15] Duchon, J. (1977). *Splines minimizing rotation-invariant semi-norms in Sobolev spaces*. Berlin, Heidelberg: Springer Berlin Heidelberg, 1977: 85-100

[16] ZONA Technology, inc. (2008). *ZAERO Theoretical Manual Version 8.2*. Scottsdale, AZ: ZONA Technology, inc.

[17] Xie, C and Yang, C. (2007). Surface Splines Generalization and Large Deflection Interpolation. *Journal of Aircraft*, 44(3): 1024-1026.

[18] Smith, M. J. and Hodges, D. H. and Cesnik, C. E. S. (2000). Evaluation of Computational Algorithms Suitable for Fluid-Structure Interactions. *Journal of Aircraft*, 37(2): 282-294.

[19] Wu, Z. and Chen, L. and Yang, C. and et al. (2011). Gust response modeling and alleviation scheme design for an elastic aircraft. *Sci China Tech Sci*, 41(3): 394-402.

[20] Lou, H. W. (2007). *Ordinary differential equation*. Shanghai, China: Fudan University Press.

[21] Zhong, W. and Williams, F. W. (1994). A Precise Time Step Integration Method. *Journal of Mechanical Engineering Science*, 208(6): 427-430.

COPYRIGHT STATEMENT